# Construction and characterization of the detection modules for the Muon Portal Project

F. Riggi, M. Bandieramonte, S. Billotta, A.A. Blancato, D.L. Bonanno, G. Bonanno, P.G. Fallica, S. Garozzo, P. La Rocca, F. Longhitano, D. Lo Presti, D. Marano, O. Parasole, C. Pugliatti, S. Riggi, G. Romeo, M. Romeo, G. Santagati, G.V. Russo

***Abstract*—The Muon Portal Project [1] is a joint initiative between research and industrial partners, aimed at the construction of a real size detector protoype (6 x 3 x 7 $m^3$) for the inspection of containers by the muon scattering technique, devised to search for hidden high-Z fissile materials and provide a full 3D tomography of the interior of the container in a scanning time of the order of minutes. The muon tracking detector is based on a set of 48 detection modules (size 1 m x 3 m), each built with 100 extruded scintillator strips, so as to provide four X-Y detection planes, two placed above and two below the container to be inspected. Two wavelength shifting (WLS) fibres embedded in each strip convey the emitted photons to Silicon Photomultipliers (SiPM) which act as photosensors. After a research and development phase, which led to the choice and test of the individual components, the construction of the full size detector has already started. The paper describes the results of the mass characterization of the photosensors and the construction and test measurements of the first detection modules of the Project.**

## I. Introduction

Cargo containers, which are now a standard way of transporting goods, circulate worldwide, with an estimate of about 200 million containers transported each year through the custom borders of many countries. They are in principle potential sources of small quantities of hidden nuclear material, such as fissile elements. Traditional systems based on X-rays inspection can hardly be employed to signal their presence, since the X-rays energy or dose required would be too high in order to penetrate big cargos and result in a significant image of the hidden volume. As an alternative to traditional detection methods, it has been long suggested [2] to employ the scattering process of the secondary cosmic muons, which strongly depends on the atomic number of the traversed material, hence particularly sensitive to high-Z fissile elements (U, Pu) or to possible shielding material (Pb). A detection system employing such technique (muon tomography) would be based on a large area muon detector, to reconstruct the muon tracks with good angular resolution, over different (at least four) detection planes.

Reconstruction and visualization algorithms may be then applied to produce a tomographic image of the container volume, able to signal the presence of hidden, high-Z materials against a large background originating from low- and medium-Z objects.

Due to the flux of secondary cosmic muons at the sea level, a large number of muon tracks - of the order of a thousands per second - are expected to cross the volume of a container, thus producing in a few minutes enough collected events to reconstruct a tomographic image with good precision, compatible with the requirements of the loading and unloading cargo procedures.

Different Projects have been exploited over the past years, aiming at building prototype detectors for muon tomography [3], [4], [5], [6], [7], [8]. They differ in the sensitive area and in the details of the detection technique employed. A new Project was recently started by the Muon Portal Collaboration [1] with the goal to build a real size detector (18 $m^2$ sensitive area for each plane) with all potential features to be used in a real situation to probe the interior of a standard 20' container. The main parameters of the design of such setup, together with the instrumentation required, are described in Sect. 2. A considerable amount of simulations and experimental tests on the individual components (scintillators, WLS fibres, photosensors, front-end electronics,...) have been already done. Different reconstruction and visualization algorithms have been implemented and have demonstrated the feasibility of this Project with the possibility of reaching enough information in a reasonable amount of time to reconstruct the tomographic image with the required precision and resolution. Several papers have recently described specific aspects of the Project [9], [10], [11], [12], [13], [14], [15], [16], [17], [18], [19], [20].

This paper is mainly concerned with the construction and characterization of the detection modules within the Muon Portal Project. Sect. 3 is devoted to the mass characterization of the photosensors, while Sect. 4 describes the construction and experimental tests carried out on the first detection modules.

## II. The Muon Portal Project

### A. Geometrical and Mechanical Structure of the Muon Portal

The detection setup is based on four XY position-sensitive physical planes, two placed above and two below the container volume to be inspected (see Fig.1).

The overall size of the detector fits that of a real TEU (Twenty-foot Equivalent Units) container, namely 6 m $\times$ 3 m $\times$ 3 m. For a suitable implementation of the detection setup,

A.A. Blancato, D.L. Bonanno, P. La Rocca, F. Longhitano, D. Lo Presti, O. Parasole, C. Pugliatti, F. Riggi, G.V. Russo, G. Santagati, are with the Dipartimento di Fisica e Astronomia, Università di Catania and INFN, Catania, Italy.

M. Bandieramonte, S. Billotta, G. Bonanno, S. Garozzo, D. Marano, S. Riggi and G. Romeo are with INAF, Osservatorio Astrofisico di Catania, Italy

P.G. Fallica and M. Romeo are with STMicroelectronics, Catania, Italy.

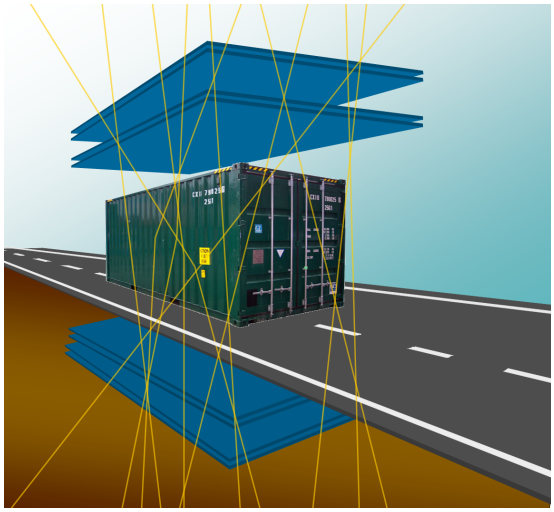

Fig. 1. Schematic view of the detector prototype for inspection of real size containers by the muon tomography technique. Four X-Y detection planes are located above and below the container, to provide track reconstruction of the cosmic muons before and after traversing the volume to be inspected.

each physical plane is made by 6 modules (1 m $\times$ 3 m each) in a proper geometry, such as to cover both the X- and the Y-coordinates by the same type of modules, without leaving any dead area between close modules. The detector will be constituted by a total of 48 modules.

A customized mechanical structure provides a suitable support for the detector planes, yet minimizing the material budget traversed by the cosmic muons (Fig.2), and allowing to position the planes at realistic distances between them (about 7 m between the top and bottom planes, with distances of about 1.5 m between each couple of tracking planes).

### *B. The detection modules*

Each of the 48 detection modules is segmented into 100 strips of extruded plastic scintillator ($1\times1 \times 300$ cm$^3$), with two wavelength-shifting (WLS) fibres embedded in each strip, to transport the photons to the photosensors placed at one of the fibre ends. The overall number of channels (fibres and photosensors) is then 9600.

After a series of experimental tests carried out on several prototypes of scintillator strips and WLS fibres from different suppliers, the final design of the detector makes use of scintillator strips from Amcrys [21] with two embedded WLS Y11 1 mm Kuraray [22] fibres.

Extensive tests of the individual strips and WLS fibres have been done and are reported in a previous paper [18].

A spatial resolution in the order of a few mm is required for all planes, in order to provide good tracking capabilities for the incoming charged particles, reconstruct their trajectories above and below the container and evaluate the amount of scattering suffered by each track.

### *C. Electronic Readout and Data Acquisition*

Taking into account the number of modules and the required granularity to achieve a reasonable space and angular resolution, a large number of channels (9600) is in principle required for such detector. A compression technique within each module (100 strips) is envisaged in our Project, in order to reduce such number to a suitable level for the electronics and data acquisition. This is achieved by the use of two WLS fibres running along the same strip (for a total of 9600 WLS fibres) and going to an equal number of SiPMs. The logical output from different photosensors is then properly combined in groups of ten, resulting in 20 channels per module. Their combination is able to identify the interested strip inside each module.

Fig. 2. Mechanical structure of the detector prototype. Four XY detection planes (18 m$^2$ each) are to be installed on this structure, with a relative distance of about 7 m between the top and bottom planes.

The front-end electronics is based on the use of MAROC3 chips (64 channels each), a fast shaping and a common threshold. Real-time boards based on FPGA FlexRIO are used, with a sampling rate up to 250 MHz.

This allows to select coincident events on the four XY planes, with a huge reduction of the spurious counting due to the relatively high dark count rate of the SiPMs.

### *D. Reconstruction and imaging algorithms*

Tracking the particles in the detector and reconstructing their trajectories involves the identification of hits and clusters in each detection plane, to be combined to identify muon tracks. Once the tracks in the upper and lower part of the detector are reconstructed, the scattering angle between the two tracks may be estimated, in order to proceed with the imaging algorithms.

A full GEANT4 replica of the complete detector has been implemented, incorporating the individual scintillator strips, the details of the mechanical structure, the walls of the

container, together with the soil below the detector. In each simulation, a set of objects of low-, medium- and high-Z material may be placed by the user inside the container volume, to understand the effect on the muon scattering and probe the capabilities of the reconstruction algorithms.

Secondary cosmic particles (muons and electrons) were modelled with realistic energy and angular distributions, as derived from CORSIKA simulations for proton-induced showers, taking into account the primary energy and angular distribution.

Several algorithms have been tested for the reconstruction of the muon scattering process. The simplest of them is based on the POCA (Point-of-Closest-Approach) method, from which a spatial distribution of the scattering centres is derived, with a weight proportional to some power of the scattering angle. The POCA algorithm makes the simplified assumption that the muon scattering occurs in a single-point. It therefore searches for the geometrical point of closest approach between the incoming and outcoming reconstructed track directions.

Such method, although of easy implementation, neglects the multiple scattering through the volume material and therefore has the drawback of providing poor-resolution images. It is quite sensitive to the presence of shield materials located above or below the potential threat and cannot localize very well materials at the volume borders. This motivated the implementation also of the log-likelihood algorithm, which is based on more realistic physical and statistical assumptions and allows to face the problems encountered with the POCA algorithm.

Clustering algorithms were tested as well, with the Friend-Of-Friend (FOF) producing the best results.

All these reconstruction algorithms were tested under different scenarios, simulating the presence of dense objects embedded in low or medium Z materials within the volume to be inspected. Detailed results on the implementation of these procedures are described elsewhere [15], [20].

## III. CHARACTERIZATION AND MASS TESTS OF THE PHOTOSENSORS

Due to the large number of channels, a natural choice for the photosensors to be employed to collect the light transported by the WLS fibres is the use of Silicon Photomultipliers (SiPM). These are compact devices, with a high gain and a low operating voltage, which have been used since several years in most demanding applications.

### A. Silicon photomultiplier technology

The silicon photomultiplier (SiPM) prototype designed for the *Muon Portal* Project had to maximize the photon detection efficiency and the cell fill factor, as well as to ensure a low cross-talk and dark count rate. Different SiPM prototypes (1 $\mathrm{mm}^2$ area), both with the *p-on-n* and *n-on-p* technologies, have been produced by STMicroelectronics before the mass production.

The layout of the final chip is based on *n-on-p* technology and embeds 4 independent round shaped SiPMs: two MUON60 type with 548 cells and 60 $\mu$m pitch, and two MUON75 type with 320 cells and 75 $\mu$m pitch. The main characteristics of the MUON60 and MUON75 SiPMs are listed in Table I.

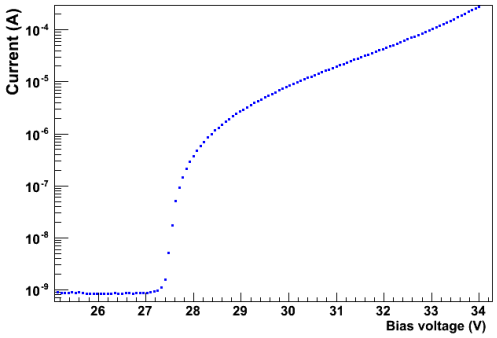


Fig. 3. I-V curve measured for one of the SiPM employed in the present Project.

The prototypes have been fully characterized (both from an electrical and optical point of view) at different temperatures and working conditions in order to choose the best device. A pulsed LED unit and a signal digitizer by CAEN were used to provide realiable measurements of various prototypes.

### B. Mass characterization of the individual devices

Since each strip is read out by two different WLS fibres, the total number of SiPMs needed for the whole detector is 9600. A batch of ∼20000 SiPMs has been produced, each encapsulated in a SMD optical package.

| **Parameter** | **MUON60** | **MUON75** |
|---|---|---|
| Sensitive area size ($\mathrm{mm}^2$) | 1.97 | 1.80 |
| Number of cells | 548 | 320 |
| Cell capacitance (fF) | 280 | 445 |
| Cell quenching resistor (kΩ) | 550 | 800 |
| Cell fill factor (%) | 67.4 | 73.8 |
| Typical breakdown voltage (V) | 27.4 | 27.4 |
| Optimal operation OV (V) | 3÷4 | 3÷4 |
| Gain | $6.8\times10^6$ | $7.6\times10^6$ |
| Typical dark current ($\mu$A) | ∼2 | ∼2 |
| Typical Dark Count Rate (MHz) | ∼2 | ∼2 |
| Optical Crosstalk (%) | 1.5 | 1.5 |
| Photon Detection Efficiency at $\Delta\lambda$ = 500-550 nm (%) | 28 | 31 |

TABLE I
FEATURES OF THE MUON60 AND MUON75 DEVICES. THE LAST 5 PARAMETERS ARE EVALUATED AT THE OPTIMAL OPERATION OVERVOLTAGE OV.

For each detection module, the SiPMs have to be optically coupled to the polished surface of the fibres and enclosed inside a light tight box, in order to be used in dark conditions and at a controlled temperature. Moreover, to improve the uniformity of the SiPMs response along the detection modules, the devices need to be sorted out into groups, depending on their breakdown voltage. SiPMs with similar characteristics are being installed in the same region of the detector in order to set, for group of 10 SiPMs, the same bias voltage and threshold level.

For this reason, an individual characterization of all the devices was necessary for their classification before the final assembling into the detection modules. A custom procedure has been implemented for the characterization of such devices. The setup is made of a black box where the device under test is placed inside a proper socket; the device is biased by a Keithley picoammeter/voltage source, that is also used to read the current from the device and transmit data to a computer. A LabVIEW program, running on a computer which communicates by RS-232 port with the Keithley device, has been developed for our purpose. A complete I-V curve is measured in an automatic way by setting the bias voltage and reading the corresponding current in the device. Starting from a bias voltage of 25 V up to 34 V in steps of 0.075 V, the program is able to find the Breakdown Voltage BV value for each SiPM under test by reading the corresponding current. As an example, in Figure 3 the I-V curve is shown for one of such devices.

The data collected for a first batch of about 4500 SiPMs have been analyzed. The selection criteria chosen has led to a rejection percentage of less than 20%, that is compatible with what expected by previous tests on prototype devices. Figure 4 shows the breakdown voltage distribution of the accepted devices.

Detailed results are reported in Ref. [19].

## IV. Construction and Tests of the Detection Modules with Cosmic Rays

### A. Assembly procedures of detection modules

To provide a two-dimensional information on the passage of cosmic muons through the various planes, a modular strategy has been employed, covering the overall surface of the tracking detector with 48 identical modules (1 m x 3 m size), placed along the X- and Y-directions. This allows a simpler construction and assembly strategy and interchangeability in case of problems. Due to their geometry, the readout is organized along three of the four sides, allowing no dead areas in the central part of the sensitive region.

Due to mechanical tolerances, before the assembly procedures all the strips were individually checked and machined with a diamond tool in order to equalize their lengths to within

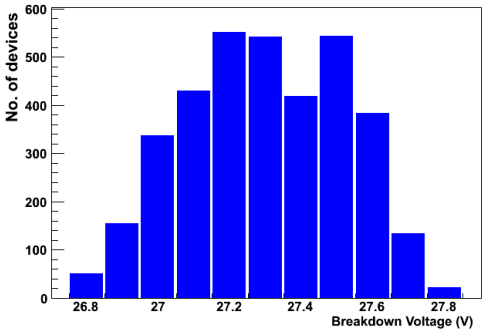


Fig. 4. Breakdown voltage distribution, measured over a sample of about 4500 devices.

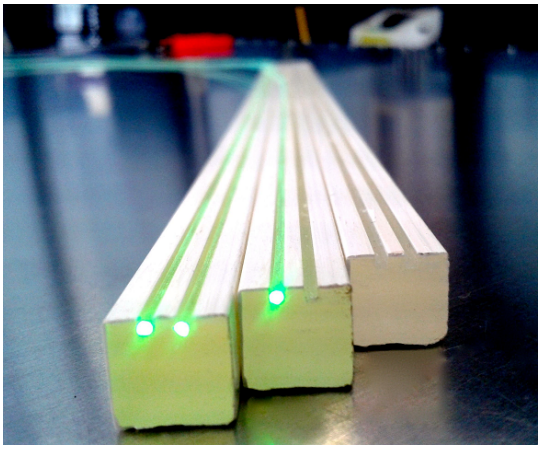

Fig. 5. Some of the 4800 extruded scintillator strips with embedded WLS fibres are shown in this picture.

approximately 0.5 mm over 3 meters. Fig.5 shows a picture of some of the strips with the WLS fibres embedded.

Each detection module is built as a sandwich which incorporates 100 extruded scintillator strips (1 cm x 1 cm x 300 cm) and 200 WLS fibres in a compact, light-tight case. Fig. 6 shows a sectional view of an individual module. During the assembly operations, scintillator strips were properly aligned on a bottom Al sheet (1 mm thickness) covered by an adehesive foil along its surface. WLS fibres are then placed along the grooves in the strips and glued at the two ends. In order to ensure the optical coupling with the photosensors, the fibres go through a plastic adapter, being glued to it and then polished by the diamond tool. Reflective Mylar tape covers all the strips and a top Al sheet covers the sandwich. The sides of the module are also covered with a reflective layer and black tape to prevent ambient light entering into it. At one end where the fibres are polished, the module is inserted in a light tight box which contains all the electronics (front-end cards with Silicon Photomultipliers, routing cards,...) together with a proper cooling system.

The assembly of each individual module required a special assembly table, equipped with a diamond tool at one end and an air pumping system to hold the module after it was assembled, to move it in a storage location before being tested and installed in the final position. The various assembly operations for a single module took about one working day. However, due to the time required for the optical glue to dry, an overall time of two days per module was required. Presently, most of the detection units have been assembled. Working

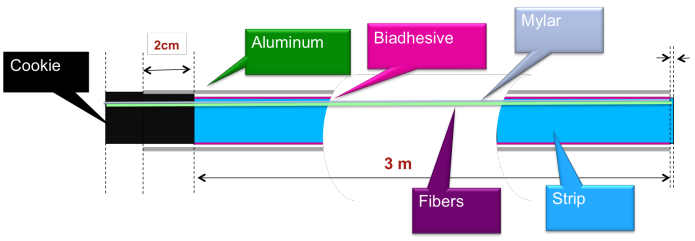


Fig. 6. Sectional view of a detection module, with its main components.

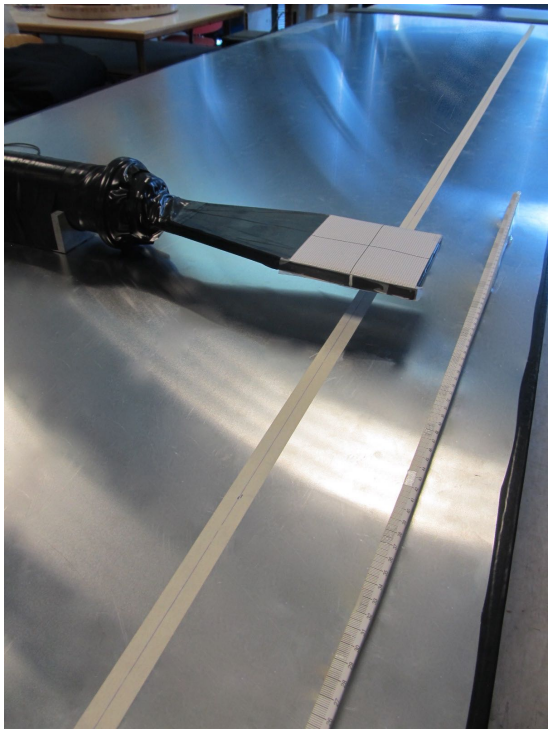

Fig. 7. One of the detection modules during a test with an external trigger scintillator.

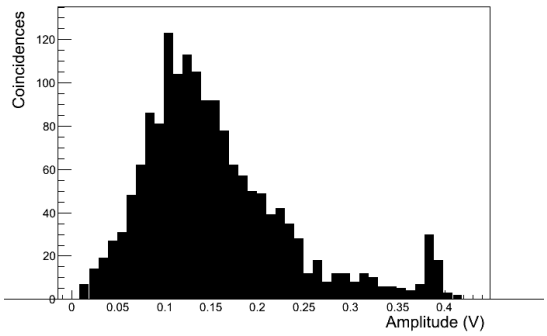


Fig. 8. Amplitude spectrum from the SiPM, measured in coincidence with an external trigger scintillator. A threshold roughly corresponding to 3 p.e. has been applied, whereas 1 p.e. corresponds to 20 mV.

tests have been performed on some of them, especially at the beginning of the construction activity, to ensure that the assembly procedure was reliable.

For this purpose, apart from inspection and visual tests, electronic tests of the module response were performed with an external trigger plastic scintillator (12 x 12 $cm^2$, 1 cm thickness, see Fig.7), placed at about 5 cm above the detection module, and moved in various positions, so as to explore a large part of the sensitive area of the module. Individual signals from Silicon photomultipliers collecting the light transported by the WLS fibres were analyzed by a digital oscilloscope in single mode or triggered by the coincident detection of a cosmic muon passing through the external scintillator. Dark current values, amplitude and time-of-flight spectra, as well as coincidence rates, were measured during such tests,

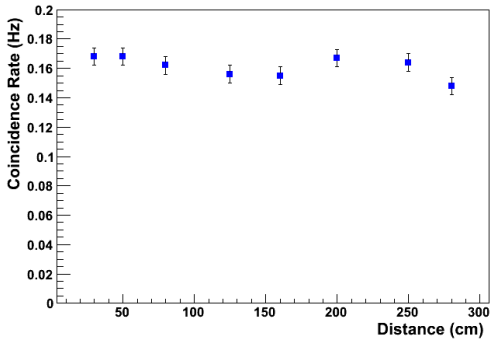


Fig. 9. Coincidence rate between one of the scintillator strips and an external trigger scintillator, as a function of its distance with respect to the photosensor.

changing the relevant parameters (bias voltage to the SiPM, discriminator threshold, location of the scintillator along the surface of the detection module,...). Preliminary calibration of the amplitude spectrum was carried out measuring the dark current signals corresponding to 1, 2, ... photoelectrons for each different bias voltage.

As an example, Fig.8 shows the amplitude spectrum for one of the channels, in coincidence with the external scintillator located at about 125 cm from the sensor, with a bias voltage of 29.5 V and a threshold of 58 mV, slightly less than 3 p.e. As it is seen, the average value of the amplitude in such conditions is around 7-8 p.e., which allows to work with a high detection efficiency, at a reasonable dark current rate even at room temperature higher than 20°, as it was during these tests, since the Peltier cells were not in operation.

Working at thresholds smaller than approximately 2-3 p.e., results in a too high dark rate in a single channel, and correspondingly a factor ten higher rate in each front-end card, due to the channel compression strategy. From about 2.5 p.e. the contribution of spurious counting rate becomes negligible with respect to the true coincidence rate due to cosmics. Fig.9 shows the observed coincidence rate between one of the module strips and the external scintillator, as a function of the SiPM threshold. An important test in our case was to check that the detection efficiency stays almost constant along the length of the strip (3 meters long). This was verified by moving the scintillator in various positions along the module (with a fixed value of the other coordinate) and measuring the coincidence rate. As an example, Fig.9 shows the result obtained at a threshold of about 2.5 p.e. Similar measurements were done on various strips and at different values of the SiPM bias voltage and discriminator level. By a proper choice of these parameters, it was checked that a constant value of the efficiency may be obtained along all the module length with a set of working conditions similar to those employed for the results shown in Fig.9. Since in the real complete detector an 8-fold coincidence is required between the eight detection planes, even smaller values of the threshold could be employed, which should allow to reach an efficiency close to 100 %. Similar tests were done on various strips (hence different WLS fibres, optical coupling and photosensor devices), to check channel to channel variations.

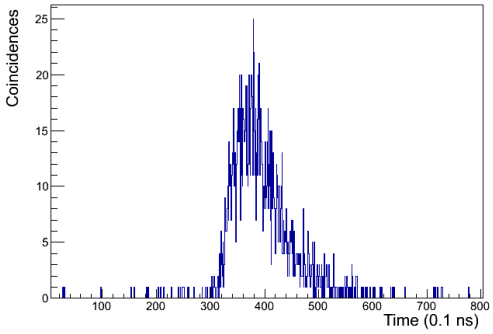


Fig. 10. Distribution of the arrival times at the SiPM, triggered by an external trigger scintillator placed at 250 cm from the photosensor.

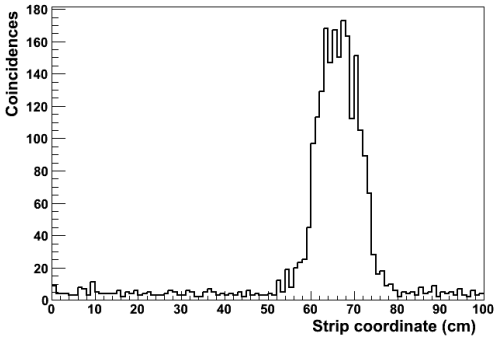


Fig. 11. Distribution of the measured coordinate along the 100 strips of a detection module, in coincidence with the external trigger scintillator.

The distribution of the arrival time of photons at the photosensors was also measured triggering with the external scintillator detector, which employs a PMT. The distribution obtained at a distance of 250 cm from the photosensor is shown in Fig.10; the value of the RMS of the peak distribution was extracted to be around 5.5 ns. Such value is the convolution of different factors: the extension of the strip length seen by cosmic muons passing through the trigger scintillator (about 20 cm), the time emission spectrum of the WLS fibres, the propagation of the optical photons along the fibre and in the scintillator, the response of the SiPM and associated electronics, and the transit time spread (TTS) of the PMT. Due to the overall time resolution, which is not specifically optimized in this detector, only a rough information about the time-of-flight between the top and bottom detection planes (about 20-30 ns) is expected, which can be mainly used to improve muon tracking and reject events with negative values of the time-of-flight.

Additional tests were done with the final design of the electronic readout system, with all components (10 front-end cards - each with 20 SiPMs - routing cards, Peltier cells,..) under conditions as close as possible to the real operating condition in the final installation. As an example, Fig.11 shows the distribution of the coordinate (along the short side of the module, 1 meter), extracted from the hit strips in coincidence with an external scintillator, placed at about 5 cm above the detection plane. The spatial resolution 1 cm/$\sqrt{12}$ was taken into account randomizing the hit (given by the strip nominal coordinate in case of single hit, or by the average of the two close strips) with a Gaussian smearing. Spurious counts which are still present along all the spectrum and under the peak mainly originate from the high value of the dark current resulting from the logical OR of ten different SiPM, with a small contribution due to real cosmic muons with very inclined tracks. This spurious contribution will become however totally negligible by the coincident detection of the muon passing through the eight (4 X and 4 Y) detection planes.

## V. Conclusions

After an intensive phase of research and development to test and choose the individual components for the construction of the detector prototype, as well as to design the mechanical structure and the electronics and readout architecture, the construction of the entire Muon Portal detector has been started and should be completed within 2015. This paper reported some details concerning the construction and testing of the detection modules, as well as the mass characterization of the individual photosensors. In its present status, most of the detection modules have been already fully prepared and some of them are already installed in the mechanical structure of the detector. Several modules were tested with cosmic rays during the construction phase, to ensure that the sequence of operations was reliable and all the channels could work with the required efficiency. The individual characterization of all the Silicon Photomultipliers has been completed, allowing to know their breakdown voltage and reject those devices not properly working before installing them on the readout cards. The overall completion of the Muon Portal detector requires in the next months the installation of all the detection modules, together with the associated front-end electronics and data routing, in order to test the overall functionality of the prototype and carry out the first commissioning tests.

## References


[1] For further details visit our Web site: *http://muoni.oact.inaf.it*
[2] Borozdin K R 2003 *Nature* **422** 277
[3] Priedhorsky W, et al., 2003 *Review of Scientific Instruments* **74** 4294
[4] Schultz L J, et al., 2004 *Nuclear Instruments and Methods in Physics Research* **A519** 687
[5] Schultz L J et al 2007 *IEEE Transactions on Image Processing* **16** 8
[6] Pesente S et al 2009 *Nuclear Instruments and Methods in Physics Research* A **A604** 738
[7] Gnanvo K et al 2011 *Nuclear Instruments and Methods in Physics Research* **A652** 16
[8] Baesso P et al 2013 *Journal of Instrumentation* **8** P08006
[9] Riggi S et al 2010 *Nuclear Instruments and Methods in Physics Research* **A624** 583
[10] Lo Presti D, et al., Proceedings of the IEEE Nuclear Science Symposium and Medical Imaging Conference (NSS/MIC), Anaheim, Oct.27-Nov.3, 2012.
[11] Riggi S, et al., Proceedings of the ECRS 2012 Conference, Moscow, 3-7 July, 2012, *J.Phys.G(Conf.Series)* **409**(2013)012046.
[12] Riggi S et al., *Nuclear Instruments and Methods in Physics Research* **A728**(2013) 59.
[13] Antonuccio V, et al., Proceedings of the ANIMMA 2013 Conference, Marseille, 2013, *Conference Record* (2013)
[14] Riggi S, et al., Proceedings of the IEEE Technology for Homeland Security (HST 2013) Conference, Boston, 2013, *Conference Record* **423**
[15] Bandieramonte M, et al., Proceedings of the IEEE Technology for Homeland Security (HST 2013) Conference, Boston, 2013, *Conference Record* **517**

[16] La Rocca P, et al., 2014 *Journal of Instrumentation* **9** C01056
[17] Pugliatti C, et al, 2014 *Journal of Instrumentation* **9** C05029
[18] Russo G V, et al, 2014 *Journal of Instrumentation* **9** P11008
[19] La Rocca P, et al., 2015 *Nuclear Instruments and Methods in Physics Research*, in press
[20] Bandieramonte M, et al., 2015 *Proceedings of the ACAT 2014 Conference*, in press
[21] Amcrys Web site, www.amcrys.com
[22] Kuraray Web site, http://www.kuraray.co.jp/en/